BJP British Journal of Pharmacology

DOI:10.1111/bph.12936
www.brjpharmacol.org

RESEARCH PAPER

Ionic mechanisms underlying the negative chronotropic action of propofol on sinoatrial node automaticity in guinea pig heart

Akiko Kojima[1], Yuki Ito[1], Hirotoshi Kitagawa[1] and Hiroshi Matsuura[2]

Departments of [1]Anesthesiology and [2]Physiology, Shiga University of Medical Science, Otsu, Shiga, Japan

Correspondence
Akiko Kojima, Department of Anesthesiology, Shiga University of Medical Science, Otsu, Shiga 520-2192, Japan. E-mail: akiko77@belle.shiga-med.ac.jp
Hiroshi Matsuura, Department of Physiology, Shiga University of Medical Science, Otsu, Shiga 520-2192, Japan. E-mail: matuurah@belle.shiga-med.ac.jp

Received
17 July 2014
Revised
16 August 2014
Accepted
9 September 2014

BACKGROUND AND PURPOSE

Propofol is a widely used intravenous anaesthetic agent, but has undesirable cardiac side effects, including bradyarrhythmia and its severe form asystole. This study examined the ionic and cellular mechanisms underlying propofol-induced bradycardia.

EXPERIMENTAL APPROACH

Sinoatrial node cells, isolated from guinea pig hearts, were current- and voltage-clamped to record action potentials and major ionic currents involved in their spontaneous activity, such as the hyperpolarization-activated cation current (I_f), T-type and L-type Ca^{2+} currents ($I_{Ca,T}$ and $I_{Ca,L}$, respectively) and the rapidly and slowly activating delayed rectifier K^+ currents (I_{Kr} and I_{Ks}, respectively). ECGs were recorded from Langendorff-perfused, isolated guinea pig hearts.

KEY RESULTS

Propofol (≥5 μM) reversibly decreased the firing rate of spontaneous action potentials and their diastolic depolarization rate. Propofol impaired I_f activation by shifting the voltage-dependent activation to more hyperpolarized potentials (≥1 μM), slowing the activation kinetics (≥3 μM) and decreasing the maximal conductance (≥10 μM). Propofol decreased $I_{Ca,T}$ (≥3 μM) and $I_{Ca,L}$ (≥1 μM). Propofol suppressed I_{Ks} (≥3 μM), but had a minimal effect on I_{Kr}. Furthermore, propofol (≥5 μM) decreased heart rates in Langendorff-perfused hearts. The sinoatrial node cell model reasonably well reproduced the negative chronotropic action of propofol.

CONCLUSIONS AND IMPLICATIONS

Micromolar concentrations of propofol suppressed the slow diastolic depolarization and firing rate of sinoatrial node action potentials by impairing I_f activation and reducing $I_{Ca,T}$, $I_{Ca,L}$ and I_{Ks}. These observations suggest that the direct inhibitory effect of propofol on sinoatrial node automaticity, mediated via multiple channel inhibition, underlies the propofol-induced bradycardia observed in clinical settings.

Abbreviations

DDR, diastolic depolarization rate; $g_{Ca,L}$, conductance of L-type Ca^{2+} current; $g_{Ca,T}$, conductance of T-type Ca^{2+} current; g_f, conductance of hyperpolarization-activated cation current; HCN, hyperpolarization-activated cyclic nucleotide-gated; I_{Ca}, voltage-dependent Ca^{2+} current; $I_{Ca,L}$, L-type Ca^{2+} current; $I_{Ca,T}$, T-type Ca^{2+} current; I_f, hyperpolarization-activated cation current; $I_{K,ACh}$, muscarinic K^+ current; I_{Kr}, rapidly activating delayed rectifier K^+ current; I_{Ks}, slowly activating delayed rectifier K^+ current; I_{to}, transient outward K^+ current; k, slope factor; MDP, maximum diastolic potential; NCX, Na^+/Ca^{2+} exchanger; SR, sarcoplasmic reticulum; τ, time constant; V_h, voltage at half-maximal activation

Tables of Links

TARGETS	
GPCRs[a]	$Ca_V1.3$
Muscarinic ACh receptors	$Ca_V3.1$
Ion channels[b]	$Ca_V3.2$
HCN1	L-type Ca^{2+} channels
HCN2	**Transporters**[c]
HCN4	Na^+/Ca^{2+} exchanger (NCX)
$Ca_V1.2$	

LIGANDS	
ACh	Nisoldipine
E-4031	Propofol
HMR1556	Tetrodotoxin

These Tables list key protein targets and ligands in this article which are hyperlinked to corresponding entries in http://www.guidetopharmacology.org, the common portal for data from the IUPHAR/BPS Guide to PHARMACOLOGY (Pawson *et al.*, 2014) and are permanently archived in the Concise Guide to PHARMACOLOGY 2013/14 ([a,b,c]Alexander *et al.*, 2013a,b,c).

Introduction

There are a number of clinical observations showing that various general anaesthetics including volatile and intravenous anaesthetics, and opioids have considerably different effects on the heart rate (Ebert *et al.*, 1995; Kanaya *et al.*, 2003; Komatsu *et al.*, 2007). We have conducted a series of studies to elucidate the ionic, cellular and neuronal mechanisms underlying changes in the heart rate during administration of sevoflurane, desflurane and remifentanil using experimental animals (Kojima *et al.*, 2012; 2013; 2014). The intravenous general anaesthetic propofol (2,6-diisopropylphenol) is widely used in the induction and maintenance of general anaesthesia and conscious sedation because of its favourable pharmacokinetic properties associated with a controllable anaesthetic state, smooth induction and fast awakening (Smith *et al.*, 1994). Clinical investigations have demonstrated that propofol evokes profound bradyarrhythmias, including sinus bradycardia, atrioventricular block and even fatal asystole (Baraka, 1988; Dorrington, 1989; Ganansia *et al.*, 1989; Tramèr *et al.*, 1997). There is evidence to indicate that the negative chronotropic action of propofol is mediated via modulation of the autonomic nervous system and/or resetting of baroreflex sensitivity in humans (Ebert *et al.*, 1992). On the other hand, propofol has been shown to decrease the heart rate in both Langendorff-perfused hearts and autonomically denervated animal models, which suggests that propofol also produces a direct cardiac effect to induce bradycardia *in vivo* (Colson *et al.*, 1988; Stowe *et al.*, 1992; Alphin *et al.*, 1995; Wu *et al.*, 1997).

Intrinsic electrical activity in neurons and heart cells is critically involved in their important physiological functions, such as controlling the consciousness level and baseline heart rate. Much attention has been paid to the modulatory effects of general anaesthetics on ion channel functions involved in neuronal and cardiac excitability in order to understand the molecular and cellular mechanisms of their effects on the neuronal and cardiac functions (Hemmings *et al.*, 2005; Franks, 2008). Propofol at clinically relevant concentrations suppresses neuronal excitability through a mechanism involving the inhibition of the hyperpolarization-activated cyclic nucleotide-gated (HCN) channels (Chen *et al.*, 2005; Ying *et al.*, 2006; Postea and Biel, 2011).

The HCN channel family compromises four distinct isoforms (HCN1 through HCN4) and is widely expressed in neurons and heart cells. The native current produced by HCNs is a hyperpolarization-activated cation current, termed either I_h in neurons or I_f in heart cells (DiFrancesco, 1993). Molecular genetic and functional studies provide evidence that I_f in the sinoatrial node, the primary pacemaker of the heart, is predominantly generated by HCN4 (Tellez *et al.*, 2006; Chandler *et al.*, 2009) and contributes to the development of slow diastolic depolarization (pacemaker depolarization), leading to the spontaneous firing of the sinoatrial node (Milanesi *et al.*, 2006; Baruscotti *et al.*, 2011). Several other ionic currents are also involved in the generation of spontaneous action potentials in the sinoatrial node (Boyett *et al.*, 2000; Dobrzynski *et al.*, 2007; Mangoni and Nargeot, 2008). These include inward currents through T-type and L-type Ca^{2+} channels ($I_{Ca,T}$ and $I_{Ca,L}$, respectively) (Mangoni *et al.*, 2003; 2006b; Baig *et al.*, 2011), as well as outward currents through the rapidly and slowly activating delayed rectifier K^+ channels (I_{Kr} and I_{Ks}, respectively) (Verheijck *et al.*, 1995; Matsuura *et al.*, 2002). In recent years, evidence has been presented to support the involvement of subsarcolemmal local Ca^{2+} releases from the sarcoplasmic reticulum (SR) in the rhythmic activity of sinoatrial node (Ca^{2+} clock mechanism; Bogdanov *et al.*, 2006; Lakatta *et al.*, 2010).

At present, little information is available regarding the effect of propofol on the intrinsic cardiac pacemaker sinoatrial node and its underlying ionic mechanisms. Our results show for the first time that supratherapeutic micromolar concentrations of propofol have a direct inhibitory effect on sinoatrial node automaticity, which appears to be ascribable to the impairment of I_f activation and a reduction in $I_{Ca,T}$, $I_{Ca,L}$ and I_{Ks}.

Methods

Isolation of sinoatrial node cells

All animal care and experimental procedures conformed to the Guide for the Care and Use of Laboratory Animals published by the US National Institutes of Health (NIH Publication No. 85-23, revised 1996) and all protocols were approved by the institution's Animal Care and Use Committee of Shiga University of Medical Science (approval number, 2013-7-14). The animals were kept under standard conditions of temperature and humidity, with a 12 h light/dark cycle (lights on at 08:00 h) and free access to food and water. A total of 38 female Hartley guinea pigs (5–8 weeks old, 280–400 g) were used in the present experiments. All studies involving animals are reported in accordance with the ARRIVE guidelines for reporting experiments involving animals (Kilkenny *et al.*, 2010; McGrath *et al.*, 2010).

Single sinoatrial node cells were obtained from the hearts of guinea pigs that had been deeply anaesthetized by an overdose of sodium pentobarbital (120 mg·kg^{-1}, i.p.), using an enzymatic dissociation procedure similar to that described previously (Matsuura *et al.*, 2002; Kojima *et al.*, 2012; 2013; 2014).

Whole-cell patch-clamp methods

Spontaneous action potentials and membrane currents were recorded using the amphotericin B-perforated and ruptured patch-clamp techniques, respectively. All recordings were conducted at 36 ± 1°C using an EPC-8 patch-clamp amplifier controlled by Patchmaster software (HEKA Elektronik, Lambrecht, Germany), as previously described (Kojima *et al.*, 2012; 2013; 2014). The current amplitude was expressed as the current density (pA·pF^{-1}), obtained by normalizing the current to the cell capacitance.

Spontaneous action potentials were recorded in normal Tyrode solution containing (in mM) 140 NaCl, 5.4 KCl, 1.8 $CaCl_2$, 0.5 $MgCl_2$, 0.33 NaH_2PO_4, 5.5 glucose and 5 HEPES (pH adjusted to 7.4 with NaOH). The pipette solution contained (in mM) 70 potassium aspartate, 50 KCl, 10 KH_2PO_4, 1 $MgSO_4$ and 5 HEPES (pH adjusted to 7.2 with KOH), to which amphotericin B (Wako Pure Chemical Industries, Osaka, Japan) was added at a final concentration of 108 μM.

I_f was recorded in normal Tyrode solution supplemented with 2 mM $NiCl_2$ and 0.5 mM $BaCl_2$, using a K$^+$-rich pipette solution containing (in mM) 70 potassium aspartate, 50 KCl, 10 KH_2PO_4, 1 $MgSO_4$, 5 ATP (disodium salt; Sigma Chemical Company, St Louis, MO, USA), 0.1 GTP (dilithium salt; Roche Diagnostics GmbH, Mannheim, Germany), 5 EGTA, 1.2 $CaCl_2$ and 5 HEPES (pH adjusted to 7.2 with KOH). I_f was measured as the difference between the instantaneous and steady-state current levels during 2000-ms hyperpolarizing steps applied from a holding potential of −40 mV. The I_f conductance (g_f) at each test potential was calculated according to the following equation: $g_f = I_f/(V_t - V_{rev})$, where I_f is current density, V_t is test potential and V_{rev} is reversal potential for I_f. The voltage dependence of I_f activation was assessed by fitting g_f to a Boltzmann equation: $g_f = g_{f,max}/\{1 + \exp[(V_t - V_h)/k]\}$, where $g_{f,max}$ is the fitted maximal conductance of I_f, V_h is the voltage at half-maximal activation and k is the slope factor.

$I_{Ca,T}$ and $I_{Ca,L}$ were recorded in Na$^+$- and K$^+$-free bath solution containing (in mM) 140 Tris-hydrochloride, 1.8 $CaCl_2$, 0.5 $MgCl_2$, 5.5 glucose and 5 HEPES (pH adjusted to 7.4 with Tris-base), to which 10 μM tetrodotoxin (Wako Pure Chemical Industries) was added to avoid the possible contamination of the voltage-gated Na$^+$ conductance. The pipette solution was a Cs$^+$-rich solution containing (in mM) 90 caesium aspartate, 30 CsCl, 20 tetraethylammonium chloride, 2 $MgCl_2$, 5 ATP (Mg salt; Sigma Chemical Company), 5 phosphocreatine (disodium salt; Sigma Chemical Company), 0.1 GTP (dilithium salt; Roche Diagnostics GmbH), 5 EGTA and 5 HEPES (pH adjusted to 7.2 with CsOH). The conductance for $I_{Ca,T}$ and $I_{Ca,L}$ was calculated at each test potential by dividing the current amplitude by the driving force for Ca^{2+} with the assumption that the reversal potential for $I_{Ca,T}$ and $I_{Ca,L}$ was the zero-current potential measured in the current–voltage relationship. The voltage-dependent activation of $I_{Ca,T}$ and $I_{Ca,L}$ was examined by constructing the conductance–voltage relationships [conductance of T-type Ca^{2+} current; $g_{Ca,T}$ or conductance of L-type Ca^{2+} current; $g_{Ca,L}$] fitted with a Boltzmann equation: $g_{Ca,T}$ (or $g_{Ca,L}$) = $g_{Ca,T,max}$ (or $g_{Ca,L,max}$)/{1 + exp[(V_h − V_t)/k]}, where $g_{Ca,T,max}$ and $g_{Ca,L,max}$ are the fitted maximal conductance for $I_{Ca,T}$ and $I_{Ca,L}$, respectively. The inactivation time course of $I_{Ca,T}$ at a test potential of −30 mV was fitted by single exponential function, while that of $I_{Ca,L}$ at −10 mV was fitted by two exponential functions.

I_{Kr} was recorded in normal Tyrode solution supplemented with 1 μM HMR1556 (Hoechst Marion Roussel, Frankfurt, Germany) and 0.4 μM nisoldipine (Sigma Chemical Company), using a K$^+$-rich pipette solution. HMR1556 at 1 μM fully inhibits I_{Ks} without affecting I_{Kr} (Thomas *et al.*, 2003).

I_{Ks} was recorded in normal Tyrode solution supplemented with 5 μM E-4031 (Wako Pure Chemical Industries) and 0.4 μM nisoldipine (Sigma Chemical Company), using a K$^+$-rich pipette solution. The voltage dependence of I_{Kr} and I_{Ks} activation was examined by fitting the tail current (I_{tail}) to a Boltzmann equation: $I_{tail} = I_{tail,max}/\{1 + \exp[(V_h - V_t)/k]\}$, where $I_{tail,max}$ is the fitted maximal tail current density. The deactivation time courses of I_{Kr} and I_{Ks} were evaluated by fitting the respective tail currents at −50 mV to single exponential function.

The muscarinic K$^+$ current ($I_{K,ACh}$) was recorded in normal Tyrode solution supplemented with 0.4 μM nisoldipine (Sigma Chemical Company), using a K$^+$-rich pipette solution without the addition of $CaCl_2$. Membrane currents were measured at a holding potential of −40 mV or during the voltage ramp protocol (dV·dt^{-1} = 1.0 V·s^{-1}), which consisted of ascending (depolarizing) phase from the holding potential (−40 mV) to +20 mV followed by a descending (hyperpolarizing) phase to −120 mV. The current–voltage relationship was determined during the descending phase. The current signals were low-pass filtered at 1 kHz, sampled at 2 kHz with an LIH-1600 AD converter (HEKA) and stored on a computer.

A previous study has measured free propofol concentration in plasma to be approximately 0.35 μM in clinical anaesthesia (Dawidowicz *et al.*, 2003), and we, therefore, examined the effect of propofol at concentrations of ≥0.3 μM on ionic currents. A concentrated stock solution of propofol (Sigma Chemical Company) was made at a concentration of 100 or 200 mM in DMSO and was diluted to 0.3–100 μM in bath solutions.

Measurement of heart rate in the Langendorff-perfused heart model

ECG was recorded from the Langendorff-perfused guinea pig hearts using a PowerLab data acquisition system and LabChart 7 software (ADInstruments, Castle Hill, Australia), as previously described (Kojima *et al.*, 2012; 2013; 2014). QT intervals were corrected (QTc) for the heart rate using Bazett's formula (Brouillette *et al.*, 2007):

$$QTc = (\text{QT interval in ms})/(\text{RR interval in s})^{1/2}$$

Sinoatrial nodal action potential simulations

A computer simulation study was conducted using the Maltsev–Lakatta rabbit sinoatrial node cell model (Maltsev and Lakatta, 2009), which was coded by simBio (Sarai *et al.*, 2006), as previously described (Kojima *et al.*, 2014). The effect of 10 μM propofol on spontaneous action potentials was simulated by incorporating the decreases in conductances of individual ionic currents (I_f, $I_{Ca,T}$, $I_{Ca,L}$, I_{Kr} and I_{Ks}) obtained by the patch-clamp experiment into the mathematical model. The sinoatrial node cell model was run for 120 s, and the last 3 s of simulation were presented.

Statistical analysis

Results are presented as the means ± SEM, with the number of animals (cell isolation) and experiments indicated by *N* and *n*, respectively. The error bars in the figures indicate SEM with *n* given in parentheses. A group size of $n = 6$ was necessary with expected differences of 10% between group means of spontaneous firing rate, a statistical power (β) of 0.8 and significance level (α) of 0.05 (StatMate Version 2.0, GraphPad Software, La Jolla, CA, USA). A group size of $n = 5$ would detect a difference of 10% between group means of maximal conductance or current amplitude for ionic currents. Statistical comparisons were made using a one-way ANOVA, followed by Dunnett's test (Prism Version 5.0; GraphPad Software). $P < 0.05$ was considered to be statistically significant.

Results

Inhibitory effect of propofol on spontaneous activity in sinoatrial node cells

Figure 1 demonstrates a typical experiment examining the effect of propofol on sinoatrial node automaticity obtained using the amphotericin B-perforated patch-clamp technique. Propofol was administered to a spontaneously active sinoatrial node cell at concentrations of 5, 10, 20 and 50 μM for approximately 4 min with a washout period of 6–8 min, and the firing rate of spontaneous action potentials was found to be decreased by each concentration of propofol in a reversible manner (Figure 1A). Figure 1B depicts the spontaneous action potentials recorded before, during the administration of propofol and after its washout, on an expanded time scale. It is evident that the action potentials are characterized by the presence of a slow diastolic depolarization phase after repolarization, which smoothly leads to the upstroke of the next action potential both in the absence and presence of propofol. There is good evidence that the slope of this diastolic depolarization, namely diastolic depolarization rate (DDR), plays an important role in determining the firing rate of spontaneous action potentials by regulating the time interval between successive action potentials (DiFrancesco, 1993). Both the spontaneous firing rate and DDR were significantly decreased by propofol at concentrations of ≥5 μM (Figure 1C, D).

Table 1 summarizes the effects of various concentrations of propofol on action potential amplitude, maximum diastolic potential (MDP), action potential duration at 50 and 90% repolarization and maximum upstroke velocity (max $dV{\cdot}dt^{-1}$). Propofol was found to significantly hyperpolarize MDP at concentrations of ≥10 μM, while having no significant effects on other parameters of the action potentials.

Impairment of I_f activation in sinoatrial node cells by propofol

To elucidate the ionic basis for the inhibitory action of propofol on spontaneous electrical activity of sinoatrial node cells, we examined the effect of propofol at concentrations of ≥0.3 μM on various membrane currents involved in sinoatrial node automaticity, namely I_f, $I_{Ca,T}$, $I_{Ca,L}$, I_{Kr} and I_{Ks} (Boyett *et al.*, 2000; Dobrzynski *et al.*, 2007; Mangoni and Nargeot, 2008).

Figure 2A shows the effects of 10 and 50 μM propofol on I_f activated at test potentials of −50 to −140 mV applied from a holding potential of −40 mV. Propofol at both concentrations decreased the amplitudes of I_f at each test potential. In addition, it is important to point out that under control conditions, I_f was appreciably activated during mild hyperpolarization to −60 and −70 mV (Figure 2B), where the slow diastolic depolarization phase occurs (see Figure 1B), and that I_f at these physiologically relevant potentials was markedly reduced by 10 and 50 μM propofol (Figure 2B, see also Figure 3C). The time course of I_f activation at −140 mV was reasonably well fitted by the sum of two exponential functions in the absence and presence of 10 and 50 μM propofol (Figure 2C). As summarized in Figure 2D–F, propofol at concentrations of ≥3 μM significantly increased the fast and slow time constants (τ_{fast} and τ_{slow}, respectively), leaving the relative amplitude of the fast component of I_f activation unaltered, thus showing that propofol slowed the activation kinetics of I_f.

We then examined the effect of propofol on the reversal potential of I_f by measuring the tail currents at various test potentials following 2000-ms hyperpolarizing step to −130 mV (Figure 3A, B). The reversal potential of I_f, which was determined from the voltage intercept of the linear regression lines for the tail currents, was not appreciably affected by 50 μM propofol (control, −24.4 ± 0.9 mV; 50 μM propofol, −24.1 ± 1.1 mV, $n = 6$; not significant), which suggests that propofol did not alter the ion selectivity of I_f to Na^+ and K^+ at their physiological concentrations under the present experimental conditions.

Figure 3C shows the conductance–voltage relationships for I_f in the absence and presence of propofol at concentrations of 0.3–50 μM, fitted with Boltzmann equation. Propofol at 10 and 50 μM significantly decreased the maximal conductance of I_f by 18.8 and 40.9% on average,

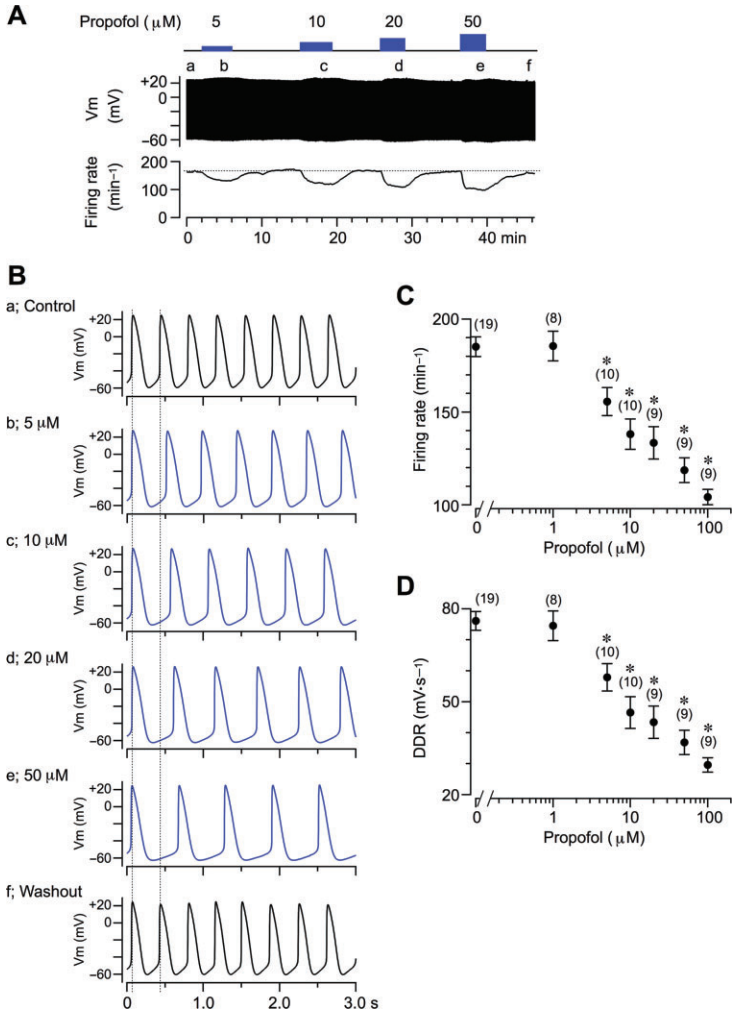

Figure 1

Inhibitory effect of propofol on the pacemaker activity of guinea pig sinoatrial node cells. (A) Continuous recordings of spontaneous action potentials during the successive application of 5, 10, 20 and 50 μM propofol (upper panel), as indicated by blue boxes. Simultaneous measurement of the firing rate of spontaneous action potentials (lower panel) plotted on the same timescale as in the action potential recordings. (B) Spontaneous action potentials on an expanded timescale recorded at time points indicated by characters (a through f) in panel A. Two dotted vertical lines denote the time interval between two successive action potentials measured under control conditions (a). (C, D) Concentration-dependent reduction of the spontaneous firing rate (C) and DDR (D) by propofol. *$P < 0.05$ compared with control.

respectively (Figure 3D). However, propofol at even lower concentrations produced significant reduction of I_f conductance at more depolarized potentials close to physiological ranges (e.g. I_f conductance at −70 mV was significantly reduced by propofol at ≥3 μM; Figure 3C, inset). Furthermore, voltage-dependent activation of I_f was shifted to more hyperpolarized potential range with increasing concentration of propofol (Figure 3E). Propofol at concentrations of ≥1 μM significantly hyperpolarized V_h of I_f activation without affecting k (Table 2).

Inhibitory effects of propofol on $I_{Ca,T}$ and $I_{Ca,L}$ in sinoatrial node cells

$I_{Ca,T}$ and $I_{Ca,L}$ were separated and identified by using different holding potentials of –90 and –60 mV and by performing subtraction of the current traces (Hagiwara *et al.*, 1988; Mangoni *et al.*, 2006b; Kojima *et al.*, 2012; 2014). Figure 4 shows the superimposed current traces for the voltage-dependent Ca^{2+} current (I_{Ca}, composed of $I_{Ca,T}$ and $I_{Ca,L}$), $I_{Ca,L}$ and $I_{Ca,T}$, recorded before and after 5 min of exposure to 50 μM propofol at various test potentials in the same sinoatrial node cell. Both $I_{Ca,T}$ and $I_{Ca,L}$ were substantially decreased by the presence of 50 μM propofol.

Figure 5A and B illustrate current–voltage relationships for $I_{Ca,T}$ and $I_{Ca,L}$, respectively, recorded in the absence and presence of propofol. $I_{Ca,T}$ and $I_{Ca,L}$ peaked at test potentials of –30 and –10 mV, respectively, under the control conditions, which were not affected by propofol. It should also be noted that, under control conditions, the peak amplitudes of $I_{Ca,T}$ and $I_{Ca,L}$ are largely similar in guinea pig sinoatrial node cells (Kojima *et al.*, 2012; 2014). Figure 5C and D illustrate the conductance–voltage relationships for $I_{Ca,T}$ and $I_{Ca,L}$, respectively, fitted with Boltzmann equation. Propofol at concentrations of ≥3 μM significantly

Table 1

Parameters of spontaneous action potentials in the absence and presence of propofol

	Control	Propofol					
	(*n* = 19, *N* = 6)	1 μM (*n* = 8, *N* = 4)	5 μM (*n* = 10, *N* = 4)	10 μM (*n* = 10, *N* = 4)	20 μM (*n* = 9, *N* = 5)	50 μM (*n* = 9, *N* = 5)	100 μM (*n* = 9, *N* = 5)
APA (mV)	83.0 ± 1.7	80.6 ± 2.5	86.8 ± 2.4	88.1 ± 2.1	84.5 ± 2.7	85.8 ± 2.4	77.4 ± 3.3
MDP (mV)	−60.0 ± 0.6	−60.6 ± 0.8	−61.2 ± 0.7	−62.4 ± 0.8*	−63.3 ± 0.8*	−63.3 ± 0.7*	−63.2 ± 0.5*
APD_{50} (ms)	102.7 ± 4.6	103.8 ± 7.4	114.0 ± 8.0	118.9 ± 7.6	103.4 ± 9.4	104.3 ± 11.0	95.0 ± 8.3
APD_{90} (ms)	161.1 ± 4.9	164.9 ± 5.8	174.2 ± 9.2	183.6 ± 9.0	171.9 ± 9.8	177.4 ± 9.5	175.1 ± 9.8
max $dV{\cdot}dt^{-1}$ ($V{\cdot}s^{-1}$)	8.3 ± 0.5	8.6 ± 0.8	10.1 ± 0.8	11.0 ± 0.7	11.0 ± 0.9	10.8 ± 1.2	8.0 ± 1.3

Data were obtained from guinea pig sinoatrial node cells and presented as mean ± SEM. Numbers of experiments (*n*) and cell isolations (*N*) are shown in parenthesis (data are from same experiments as shown in Figure 1C, D). *$P < 0.05$ compared with control.
APA, action potential amplitude; MDP, maximal diastolic potential; APD_{50}, action potential duration at 50% repolarization; APD_{90}, action potential duration at 90% repolarization; max $dV{\cdot}dt^{-1}$, maximal rate of rise of the action potential.

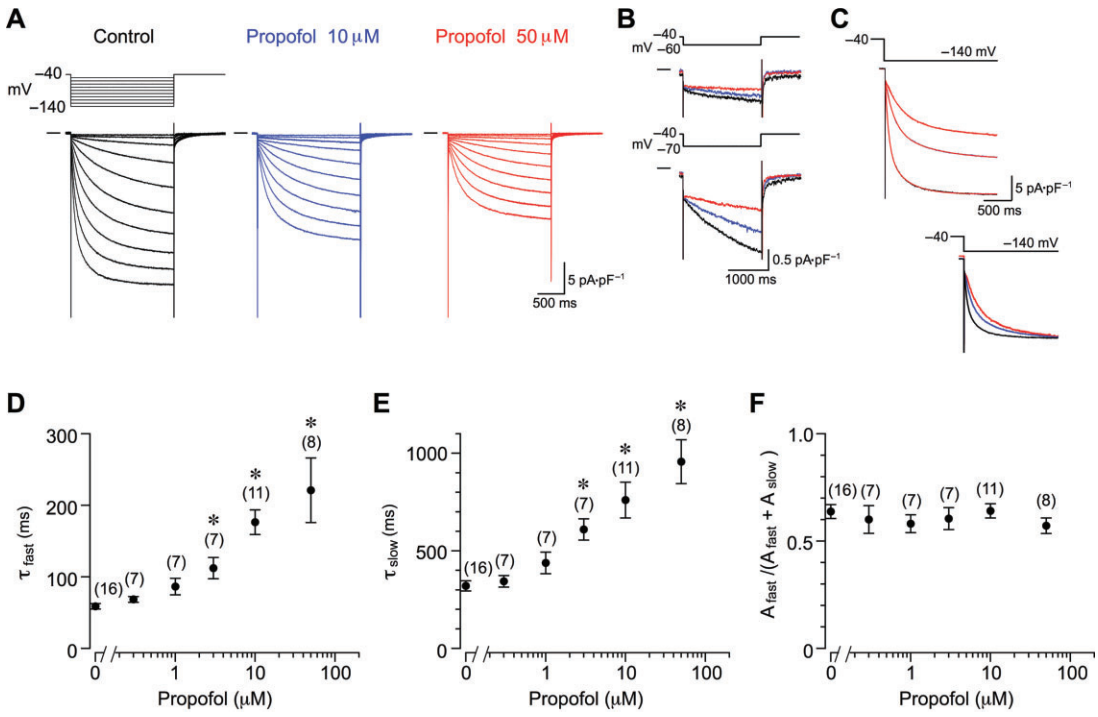

Figure 2

Slowing of I_f activation in guinea pig sinoatrial node cells by propofol. (A) Superimposed current traces of I_f during 2000-ms hyperpolarizing steps to −50 to −140 mV given from a holding potential of −40 mV. Propofol at 10 and 50 μM was applied in a cumulative manner (each concentration for approximately 5 min). It was confirmed in different sets of experiments that the inhibitory effect of 50 μM propofol on I_f, repetitively (every 8 s) activated by 2000-ms hyperpolarizing steps to −130 mV, reached a steady-state level within 2 min after application and was fully reversed within 3 min after washout (data not shown). (B) Superimposed I_f activated during 2000-ms hyperpolarizing steps to −60 mV (upper panel) and −70 mV (lower panel), before (black traces) and during application of 10 (blue) and 50 μM (red) propofol. (C) I_f activated during 2000-ms hyperpolarizing steps to −140 mV (dotted points), before and during application of 10 and 50 μM propofol, was fitted with sum of two exponential functions (continuous curve). Inset shows superimposed I_f recorded at −140 mV before and during application of 10 and 50 μM propofol, where the peak amplitude of I_f in the presence of propofol was normalized to that of I_f in control to clarify the slowing of the current activation. (D, E) Time constants for the fast (τ_{fast}, D) and slow (τ_{slow}, E) components of I_f activation at −140 mV in the absence and presence of propofol at concentrations of 0.3–50 μM. (F) The relative amplitude of the fast component of I_f activation at −140 mV in the absence and presence of propofol at concentrations of 0.3–50 μM. *$P < 0.05$ compared with control.

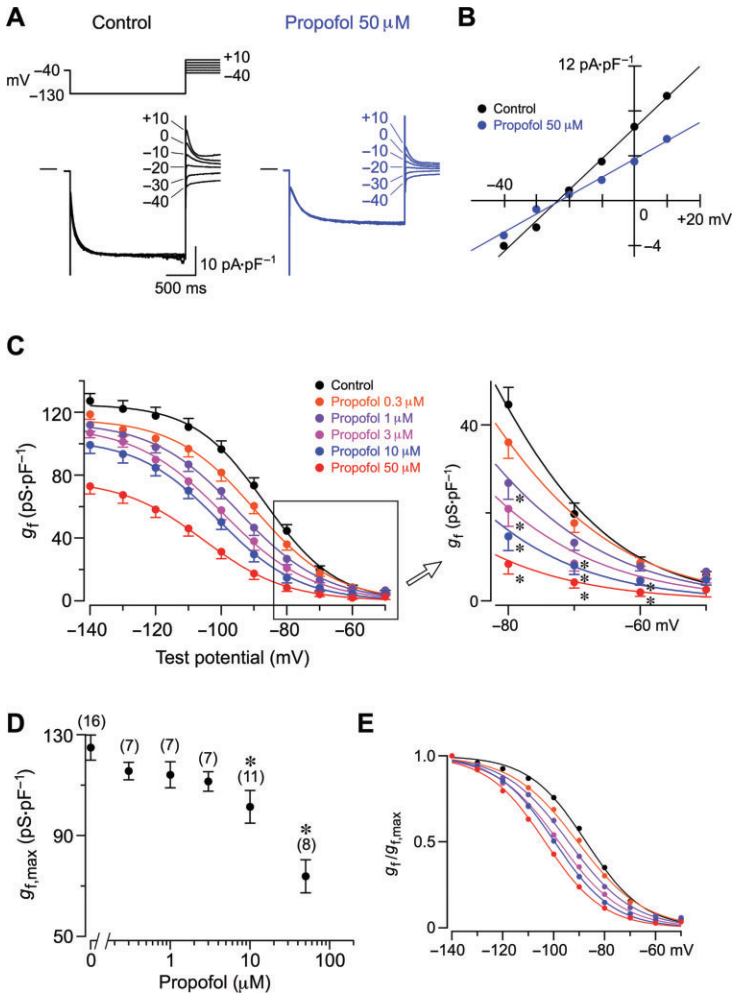

Figure 3

Inhibitory effects of propofol on I_f conductance in guinea pig sinoatrial node cells. (A) Tail currents of I_f recorded at various test potentials of +10 to −40 mV following 2000-ms hyperpolarizing steps to −130 mV, before and 5 min after exposure to 50 μM propofol. (B) Current–voltage relationships for I_f tail currents at test potentials of +10 to −40 mV, obtained from the data shown in panel A. Straight lines represent the linear regression for each condition. (C) Conductance–voltage relationship for I_f constructed using the reversal potential of −24 mV in the absence and presence of propofol at concentrations of 0.3–50 μM, fitted with Boltzmann equation. Inset shows I_f conductance at −60, −70 and −80 mV on an expanded scale. (D) Effects of propofol on the fitted maximal conductance of I_f ($g_{f,max}$), obtained using Boltzmann fitting of the data shown in the panel C. (E) Normalized I_f conductance–voltage relationships, where I_f conductance at each test potential in the absence and presence of propofol was normalized with reference to its fitted maximal conductance ($g_{f,max}$) under each condition. Note that voltage dependence of I_f activation was shifted to hyperpolarized potentials by the presence of propofol. *P < 0.05 compared with control.

decreased the maximal conductance of $I_{Ca,T}$ (Figure 5E), while propofol at ≥1 μM significantly reduced the maximal conductance of $I_{Ca,L}$ (Figure 5F). The voltage dependences for the activation of $I_{Ca,T}$ and $I_{Ca,L}$ were not significantly affected by propofol, as judged from the values for V_h and k (Table 2). In addition, propofol at any concentrations did not significantly affect inactivation time constants for $I_{Ca,T}$ and $I_{Ca,L}$ (Table 3).

Effects of propofol on I_{Kr} and I_{Ks} in sinoatrial node cells

Previous studies have clearly demonstrated that propofol at a concentration of 100 μM inhibits I_{Ks} without appreciably affecting I_{Kr} in guinea pig ventricular myocytes and rabbit sinoatrial node cells (Heath and Terrar, 1996a; Lei and Brown, 1996). We therefore examined the effects of propofol at concentrations of ≤100 μM on I_{Kr} and I_{Ks} in guinea pig sinoatrial node pacemaker cells.

Figure 6A depicts the superimposed current traces during 250-ms depolarizing steps to 0 mV applied from a holding potential of −50 mV under control conditions (a) and during cumulative application of 10 (b), 50 (c) and 100 μM (d) propofol, and after subsequent addition of 5 μM E-4031 (e). I_{Kr} was determined as the E-4031-sensitive difference current in these experiments. Figure 6B demonstrates I_{Kr} at a test potential of 0 mV under control conditions (a–e) and in the presence of 10 (b–e), 50 (c–e) and 100 μM (d–e) propofol. Single exponential fit of I_{Kr} tail current showed that the deac-

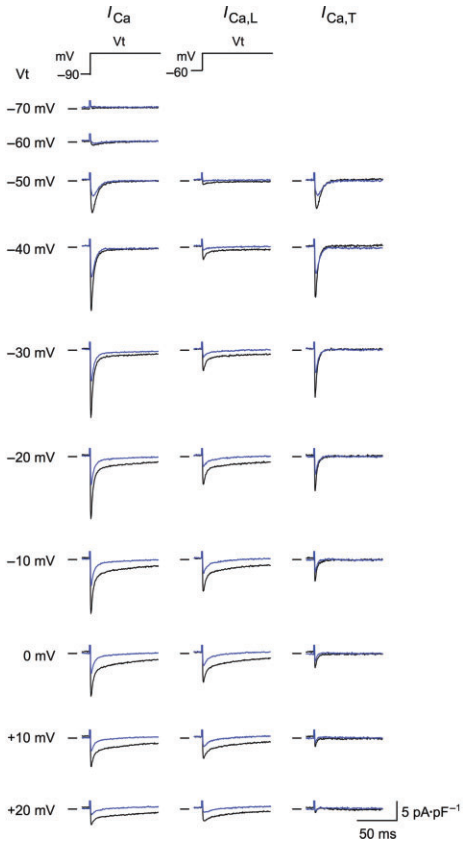

Figure 4

Effects of propofol on $I_{Ca,T}$ and $I_{Ca,L}$ in guinea pig sinoatrial node cells. Superimposed current traces for I_{Ca} (composed of $I_{Ca,T}$ and $I_{Ca,L}$), $I_{Ca,L}$ and $I_{Ca,T}$ at various test potentials, recorded before (black traces) and 5 min after (blue traces) the application of 50 μM propofol. The cell membrane was initially depolarized from a holding potential of −90 mV to test potentials of −70 through +40 mV to activate I_{Ca} (=$I_{Ca,T}$ + $I_{Ca,L}$) and was then depolarized from a holding potential of −60 mV to test potentials of −50 through +40 mV to elicit $I_{Ca,L}$. $I_{Ca,T}$ was obtained by digitally subtracting $I_{Ca,L}$ from I_{Ca} at each test potential. The duration of each depolarizing step was 200 ms, and the amplitude of $I_{Ca,T}$ and $I_{Ca,L}$ was measured as the peak inward current level. It was confirmed in different sets of experiments that the inhibitory effect of 50 μM propofol on $I_{Ca,T}$ (activated by depolarization from −90 to −50 mV every 8 s) and $I_{Ca,L}$ (activated by depolarization from −60 to −10 mV every 8 s) reached a steady-state level within 2 min after application and was largely reversed within 5 min after washout (data not shown).

tivation kinetics of I_{Kr} at −50 mV was not appreciably affected by propofol (Figure 6B and Table 3). The amplitudes of I_{Kr} tail currents at test potentials of −40 through +50 mV in the absence and presence of propofol were plotted and fitted with Boltzmann equation (Figure 6C). There were no significant differences in the maximal amplitude of I_{Kr} tail currents, as estimated by Boltzmann fit, in the absence and presence of propofol (Figure 6D). Furthermore, voltage dependence for I_{Kr} activation was not affected by propofol (Table 2).

Figure 7A shows superimposed I_{Ks} activated during 2000-ms depolarizing steps to test potentials of −40 to +50 mV, before and during the successive application of 10, 50 and 100 μM propofol, and after the washout of 100 μM propofol. Figure 7B summarizes the effects of propofol at concentrations of 0.3–100 μM on the current–voltage relationships for I_{Ks} tail currents measured at −50 mV, fitted with Boltzmann equation. The fitted maximal amplitude of I_{Ks} tail current ($I_{Ks,max}$) was significantly reduced by propofol at ≥3 μM (Figure 7C). However, neither voltage dependence of I_{Ks} activation nor deactivation kinetics of I_{Ks} was significantly affected by propofol (Tables 2 and 3).

Lack of $I_{K,ACh}$ activation in sinoatrial node cells by propofol

Stimulation of the M_2-muscarinic receptor activates $I_{K,ACh}$, which contributes to the hyperpolarization of MDP and slowing of automaticity in sinoatrial node cells (Boyett *et al.*, 2000). In addition, previous competitive binding assays provide evidence that propofol directly binds to the M_2-muscarinic receptor in the cardiac cell membrane (Alphin *et al.*, 1995; Yamamoto *et al.*, 1999). We therefore examined whether or not propofol activates $I_{K,ACh}$ to decelerate the spontaneous activity of sinoatrial node cells (Figure 8). Bath application of 100 μM propofol had no effect on the membrane current during voltage ramp between +20 and −120 mV, whereas the subsequent application of 1 μM ACh to the same sinoatrial node cell robustly activated $I_{K,ACh}$, as judged from its current–voltage relationship exhibiting a moderate inwardly rectifying property with a reversal potential (around −85 mV) near equilibrium potential for K^+ in the present experimental conditions (−88.4 mV). Essentially similar results were obtained in the other sinoatrial node cells using 10 μM (n = 3) and 100 μM (n = 7) of propofol. These observations indicate that the propofol-induced slowing of spontaneous activity accompanied by hyperpolarization of MDP is independent of $I_{K,ACh}$.

Negative chronotropic effect of propofol in the Langendorff-perfused guinea pig heart

We next examined the effect of propofol at concentrations of 5–100 μM on ECG recorded from the Langendorff-perfused heart model (Figure 9), in which the neural and humoural influences are mostly abolished (Young *et al.*, 2001). Propofol reversibly decreased the heart rate in a concentration-dependent manner without significantly affecting QTc interval (Figure 9B, C). Similar results have previously been reported by other investigators (Cacheaux *et al.*, 2005). It should also be noted that in guinea pig ventricular myocytes, propofol inhibits both $I_{Ca,L}$ (Yang *et al.*, 1996) and I_{Ks} (Heath and Terrar, 1996a), which is expected to shorten and prolong ventricular repolarization, respectively. This multichannel blocking property of propofol may result in insignificant changes in QTc interval (Figure 9C). Atrial and ventricular premature contractions, ventricular tachycardia and ventricular fibrillation were not observed during experimental protocol of propofol administration (data not shown).

Computer simulation for propofol effect on spontaneous automaticity in sinoatrial node cell

Our final investigation explored the implication of propofol-induced changes in ionic currents in its negative chrono-

Table 2

Voltage dependence of activation for I_f, $I_{Ca,T}$, $I_{Ca,L}$, I_{Kr} and I_{Ks} in the absence and presence of propofol

		Control	Propofol (μM)					
			0.3	1	3	10	50	100
I_f	V_h (mV)	−86.8 ± 1.3	−89.9 ± 2.0	−95.1 ± 2.6*	−99.3 ± 3.5*	−99.8 ± 2.4*	−102.9 ± 2.5*	
		(n = 16, N = 5)	(n = 7, N = 2)	(n = 7, N = 2)	(n = 7, N = 2)	(n = 11, N = 5)	(n = 8, N = 3)	
	k (mV)	10.5 ± 0.5	12.0 ± 0.7	12.3 ± 0.6	12.3 ± 0.7	10.8 ± 0.7	10.9 ± 0.8	
		(n = 16, N = 5)	(n = 7, N = 2)	(n = 7, N = 2)	(n = 7, N = 2)	(n = 11, N = 5)	(n = 8, N = 3)	
$I_{Ca,T}$	V_h (mV)	−44.9 ± 1.0	−44.6 ± 0.6	−44.1 ± 0.7	−43.9 ± 0.8	−46.2 ± 1.2	−47.7 ± 2.2	
		(n = 15, N = 4)	(n = 6, N = 2)	(n = 6, N = 2)	(n = 6, N = 2)	(n = 6, N = 2)	(n = 6, N = 2)	
	k (mV)	5.4 ± 0.4	5.7 ± 0.2	5.5 ± 0.2	5.8 ± 0.2	6.3 ± 0.6	5.6 ± 0.7	
		(n = 15, N = 4)	(n = 6, N = 2)	(n = 6, N = 2)	(n = 6, N = 2)	(n = 6, N = 2)	(n = 6, N = 2)	
$I_{Ca,L}$	V_h (mV)	−29.3 ± 1.4	−27.2 ± 1.7	−27.8 ± 1.2	−27.4 ± 1.8	−30.5 ± 1.8	−30.2 ± 2.9	
		(n = 15, N = 4)	(n = 6, N = 2)	(n = 6, N = 2)	(n = 6, N = 2)	(n = 6, N = 2)	(n = 6, N = 2)	
	k (mV)	8.4 ± 0.2	8.2 ± 0.3	8.1 ± 0.1	8.2 ± 0.3	9.0 ± 0.4	8.6 ± 0.3	
		(n = 15, N = 4)	(n = 6, N = 2)	(n = 6, N = 2)	(n = 6, N = 2)	(n = 6, N = 2)	(n = 6, N = 2)	
I_{Kr}	V_h (mV)	−21.8 ± 1.4				−22.9 ± 1.5	−25.2 ± 1.6	−24.0 ± 1.2
		(n = 9, N = 3)				(n = 6, N = 2)	(n = 5, N = 2)	(n = 7, N = 3)
	k (mV)	7.2 ± 0.5				8.5 ± 0.5	7.9 ± 0.7	7.2 ± 0.6
		(n = 9, N = 3)				(n = 6, N = 2)	(n = 5, N = 2)	(n = 7, N = 3)
I_{Ks}	V_h (mV)	9.5 ± 1.2	8.2 ± 1.4	8.0 ± 1.4	8.0 ± 1.4	12.5 ± 1.3	11.2 ± 2.3	12.8 ± 2.4
		(n = 13, N = 3)	(n = 6, N = 2)	(n = 6, N = 2)	(n = 6, N = 2)	(n = 7, N = 2)	(n = 6, N = 2)	(n = 6, N = 2)
	k (mV)	13.0 ± 0.4	11.9 ± 0.3	12.5 ± 0.1	12.5 ± 0.3	14.4 ± 0.7	14.7 ± 0.9	14.5 ± 1.7
		(n = 13, N = 3)	(n = 6, N = 2)	(n = 6, N = 2)	(n = 6, N = 2)	(n = 7, N = 2)	(n = 6, N = 2)	(n = 6, N = 2)

Data were obtained from guinea pig sinoatrial node cells and presented as mean ± SEM. Numbers of experiments (n) and cell isolations (N) are shown in parenthesis. *P < 0.05 compared with control.
V_h, voltage at half-maximal activation; k, slope factor.

tropic action, using the Maltsev–Lakatta model of rabbit sinoatrial node cell (Maltsev and Lakatta, 2009). As demonstrated in Figure 10, the firing rate of spontaneous action potentials of sinoatrial node in the computer model was decreased by 3.8%. Although there is some difference in the degree of reduction of the spontaneous firing rate between the experimental (25.4%, Figure 1) and simulation (3.8%, Figure 10) studies, the computer simulation using the Maltsev–Lakatta model can, at least qualitatively, reproduce the negative chronotropic action of propofol on the sinoatrial node cells. Previous clinical investigations have reported that the heart rate was reduced by approximately 5–50% during propofol administration in humans (Cullen *et al.*, 1987; Baraka, 1988; Kanaya *et al.*, 2003).

Discussion

The propofol-induced deceleration of the sinoatrial node automaticity was typically accompanied by depression of diastolic depolarization in spontaneous action potentials (Figure 1). It is generally accepted that diastolic depolarization is produced by a complex but coordinated interaction of multiple inward and outward ionic currents, such as I_f, $I_{Ca,T}$, $I_{Ca,L}$, I_{Kr} and I_{Ks} (Boyett *et al.*, 2000; Dobrzynski *et al.*, 2007; Mangoni and Nargeot, 2008). The present voltage-clamp experiments reveal that propofol impairs I_f activation by hyperpolarizing the voltage-dependent activation (≥1 μM; Figure 3E and Table 2), slowing the activation kinetics (≥3 μM; Figure 2D, E) and reducing the maximal conductance (≥10 μM; Figure 3D). It is important to point out that the combined effects of these functional impairments lead to a substantial reduction of I_f activation at a membrane potential of –60 mV (Figures 2B and 3C), where slow diastolic depolarization occurs (Figure 1B). Because there is experimental evidence that I_f contributes to the slow diastolic depolarization and pacemaker activity in guinea pig sinoatrial node cells (Kojima *et al.*, 2012), it is reasonable to propose that these functional impairments of I_f associated with current reduction are responsible, at least partly, for the propofol-induced deceleration of the spontaneous activity in sinoatrial node cells. In addition, because the pharmacological blockade of I_f has been shown to hyperpolarize MDP in sinoatrial node cells (Gao *et al.*, 2010), it seems likely that the propofol (≥10 μM)-induced hyperpolarization of MDP (Table 1) is ascribable to the reduction of the inward (depolarizing) current carried by I_f.

Previous studies have demonstrated that the effect of propofol on I_h, the neuronal equivalent of cardiac I_f, varies in

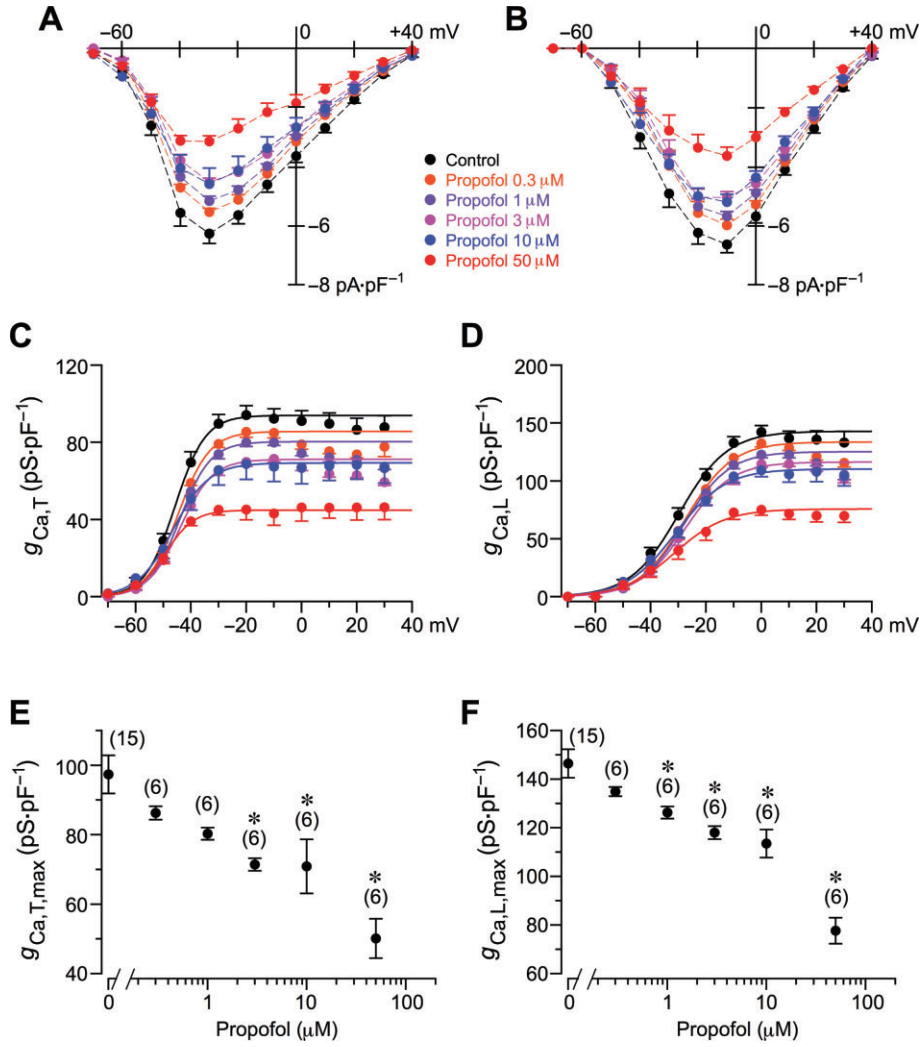

Figure 5

Inhibition of $I_{Ca,T}$ and $I_{Ca,L}$ conductances in guinea pig sinoatrial node cells by propofol. (A, B) Current–voltage relationships for $I_{Ca,T}$ (A) and $I_{Ca,L}$ (B) in the absence and presence of propofol at concentrations of 0.3–50 μM. (C, D) Conductance–voltage relationships for $I_{Ca,T}$ (C) and $I_{Ca,L}$ (D) in the absence and presence of propofol, fitted with Boltzmann equation. (E, F) Effects of propofol on the fitted maximal conductance of $I_{Ca,T}$ ($g_{Ca,T,max}$, E) and $I_{Ca,L}$ ($g_{Ca,L,max}$, F), obtained using Boltzmann fitting of the data shown in panels C and D, respectively. *P < 0.05 compared with control.

different neuronal cell types (Chen *et al.*, 2005; Ying *et al.*, 2006). Whereas propofol inhibits I_h in cortical pyramidal neurons, where there is a relatively high expression of HCN1, by hyperpolarizing the voltage-dependent activation, decreasing the maximal current amplitude and slowing the activation kinetics, propofol only slows the activation kinetics of I_h in thalamocortical neurons, where HCN2 predominates (Chen *et al.*, 2005). These differences in the sensitivity of neuronal I_h to inhibition by propofol have been proposed to arise from the isoform-dependent inhibitory action of propofol on HCN channels. Heterologous expression experiments have shown that propofol preferentially suppresses HCN1 channels, while having only a small or minimal effect on HCN2 and HCN4 channels (Cacheaux *et al.*, 2005; Chen *et al.*, 2005; Tibbs *et al.*, 2013). The present experiments, however, demonstrate that micromolar concentrations of propofol significantly impair the electrophysiological function of I_f and thereby reduce its current amplitude in sinoatrial node cells (Figures 2 and 3), where HCN4 is expected to underlie the major fraction of HCN isoforms with additional contributions of HCN1 and/or HCN2 (Tellez *et al.*, 2006; Chandler *et al.*, 2009). It is likely that the native I_f in sinoatrial node cells is more profoundly impaired by propofol than predicted from the experimental results obtained by heterologously expressed HCN4 channels in *Xenopus* oocytes (Cacheaux *et al.*, 2005). This may be due at least partly to the absorption of hydrophobic small molecules, such as propofol, by the vitelline membrane and the viscous yolk of the *Xenopus* oocytes.

The degree of $I_{Ca,L}$ inhibition by propofol is qualitatively similar in sinoatrial node cells (Figures 4 and 5) and ventricular myocytes (Yang *et al.*, 1996) of guinea pig heart. Because

Table 3

Time constants for inactivation of $I_{Ca,T}$ and $I_{Ca,L}$ or deactivation of I_{Kr} and I_{Ks} in the absence and presence of propofol

		Control	Propofol (μM)					
			0.3	1	3	10	50	100
$I_{Ca,T}$	τ (ms)	6.5 ± 0.3 (n = 15, N = 4)	6.3 ± 0.4 (n = 6, N = 2)	6.7 ± 0.6 (n = 6, N = 2)	7.0 ± 0.4 (n = 6, N = 2)	7.1 ± 0.4 (n = 6, N = 2)	7.8 ± 0.4 (n = 6, N = 2)	
$I_{Ca,L}$	τ_{fast} (ms)	4.9 ± 0.2 (n = 15, N = 4)	5.4 ± 0.3 (n = 6, N = 2)	5.5 ± 0.5 (n = 6, N = 2)	5.8 ± 0.3 (n = 6, N = 2)	5.3 ± 0.3 (n = 6, N = 2)	5.3 ± 0.7 (n = 6, N = 2)	
	τ_{slow} (ms)	75.5 ± 4.4 (n = 15, N = 4)	79.9 ± 4.7 (n = 6 N = 2)	79.8 ± 4.7 (n = 6, N = 2)	81.3 ± 4.8 (n = 6, N = 2)	78.7 ± 6.3 (n = 6, N = 2)	74.7 ± 8.5 (n = 6, N = 2)	
	$A_{fast}/(A_{fast}+A_{slow})$	0.66 ± 0.01 (n = 15, N = 4)	0.66 ± 0.02 (n = 6, N = 2)	0.65 ± 0.03 (n = 6, N = 2)	0.65 ± 0.03 (n = 6, N = 2)	0.65 ± 0.03 (n = 6, N = 2)	0.64 ± 0.03 (n = 6, N = 2)	
I_{Kr}	τ (ms)	214.1 ± 5.2 (n = 9, N = 3)				216.1 ± 9.7 (n = 6, N = 2)	221.9 ± 5.9 (n = 5, N = 2)	219.0 ± 9.0 (n = 7, N = 3)
I_{Ks}	τ (ms)	208.1 ± 8.6 (n = 13, N = 3)	206.2 ± 20.9 (n = 6, N = 2)	205.3 ± 15.8 (n = 6, N = 2)	207.7 ± 18.5 (n = 6, N = 2)	210.0 ± 5.8 (n = 7, N = 2)	192.8 ± 13.8 (n = 6, N = 2)	189.0 ± 17.3 (n = 6, N = 2)

Data were obtained from guinea pig sinoatrial node cells and presented as mean ± SEM. Numbers of experiments (n) and cell isolations (N) are shown in parenthesis. *P < 0.05 compared with control.
τ, time constant.

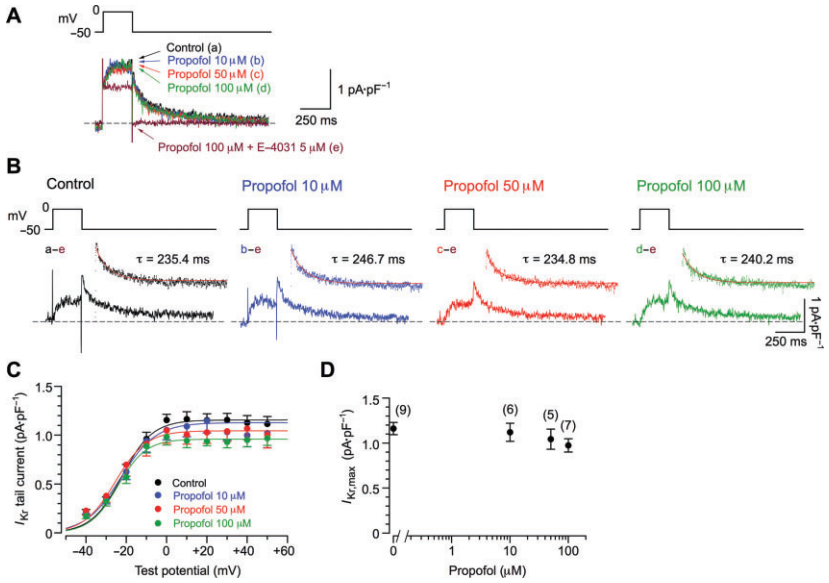

Figure 6

Effect of propofol on I_{Kr} in guinea pig sinoatrial node cells. (A) Superimposed current traces during 250-ms depolarizing steps to 0 mV from a holding potential of −50 mV, before (a) and during the administration of 10 (b), 50 (c) and 100 μM (d) propofol in a cumulative manner (each concentration for approximately 3–5 min), and 5 min after the subsequent addition of 5 μM E-4031 with 100 μM propofol (e). HMR1556 (1 μM) and nisoldipine (0.4 μM) are present in the bath throughout the experiment. (B) I_{Kr} in control (a–e) and in the presence of 10 (b–e), 50 (c–e) and 100 μM (d–e) propofol, obtained by appropriate subtraction of the data shown in panel A, as indicated. The I_{Kr} tail current in each condition (dotted points) was fitted with a single exponential function (continuous curves) with the time constant (τ) as indicated. (C) Current–voltage relationships for I_{Kr} tail currents, determined as E-4031-sensitive current, in the absence and presence of 10, 50 and 100 μM propofol. The smooth curves through the data points represent least squares fit of the Boltzmann equation. (D) Effects of propofol on the fitted maximal amplitude of I_{Kr} tail current ($I_{Kr,max}$), obtained using Boltzmann fitting of the data shown in the panel C.

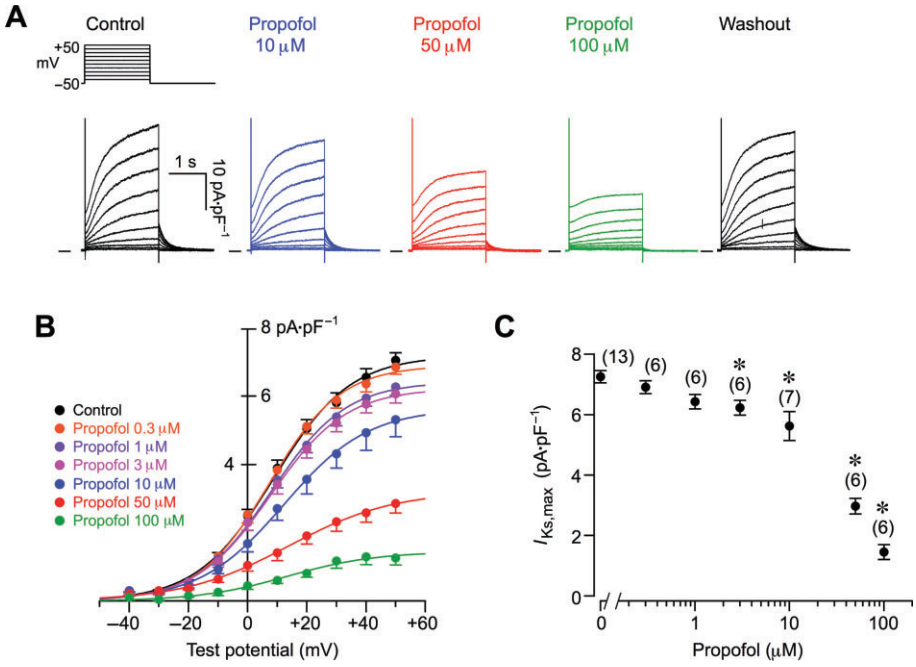

Figure 7

Inhibitory effects of propofol on I_{Ks} in guinea pig sinoatrial node cells. (A) Superimposed current traces of I_{Ks} activated by 2000-ms depolarizing voltage steps to −40 to +50 mV applied from a holding potential of −50 mV, recorded before and during exposure to increasing concentrations (10, 50 and 100 μM) of propofol for approximately 5 min at each concentration, and 5 min after washout of 100 μM propofol. It was confirmed in different sets of experiments that the inhibitory action of 50 μM propofol on I_{Ks}, repetitively (every 8 s) activated by 2000-ms depolarizing steps to +40 mV, reached a steady-state level within 2 min after the application and was fully reversed within 4 min after the washout (data not shown). (B) Current–voltage relationships for I_{Ks} tail currents in the absence and presence of propofol at concentrations of 0.3–100 μM. The smooth curves through the data points represent least squares fit of the Boltzmann equation. (C) Effect of propofol on the fitted maximal amplitude of I_{Ks} tail current ($I_{Ks,max}$), obtained using Boltzmann fitting of the data shown in the panel B. *$P < 0.05$ compared with control.

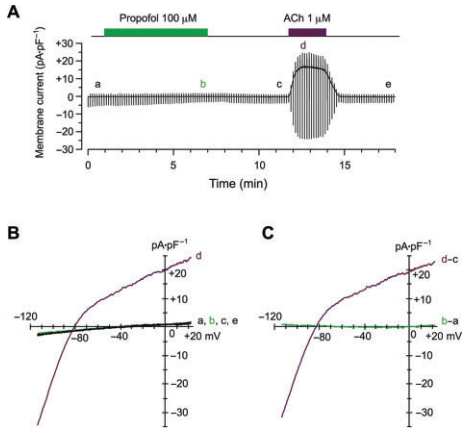

Figure 8

Lack of $I_{K,ACh}$ activation in guinea pig sinoatrial node cells by propofol. (A) Changes in membrane currents during voltage ramp protocol applied every 8 s during the applications of 100 μM propofol and 1 μM ACh, as indicated. (B) Current–voltage relationships recorded at the time points indicated by characters (a through e) in panel A. (C) Current–voltage relationships for the propofol- (b–a) and ACh-activated currents (d–c) obtained by digital subtraction of original current traces as indicated.

there is good evidence that $I_{Ca,L}$ in sinoatrial node cells and ventricular myocytes is carried by different L-type Ca^{2+} channel α-subunits (Tellez *et al.*, 2006; Mangoni and Nargeot, 2008; Chandler *et al.*, 2009), $Ca_V1.3$-based sinoatrial nodal $I_{Ca,L}$ and $Ca_V1.2$-based ventricular $I_{Ca,L}$ are both sensitive to inhibition by propofol. This study also demonstrates that propofol reduces $I_{Ca,T}$ in sinoatrial node cells (Figures 4 and 5), which is assumed to be produced by $Ca_V3.1$ and $Ca_V3.2$ (Dobrzynski *et al.*, 2007; Mangoni and Nargeot, 2008). A previous study has shown that propofol inhibits both $Ca_V3.1$ and $Ca_V3.2$ channels heterologously expressed in HEK cells without affecting the rate of current inactivation (Todorovic *et al.*, 2000), which may support the inhibitory effect of propofol on $I_{Ca,T}$ in sinoatrial node cells (Figures 4 and 5) at the molecular levels.

There are a number of studies showing that I_{Kr} and I_{Ks} represent differential sensitivity to a variety of compounds including clinical drugs. The volatile anaesthetics sevoflurane and desflurane inhibit I_{Ks} without appreciably affecting I_{Kr} in sinoatrial node cells and ventricular myocytes (Shibata *et al.*, 2004; Kojima *et al.*, 2012; 2014). Thus, the pharmacological sensitivity of I_{Kr} and I_{Ks} to the intravenous anaesthetic propofol is similar to that observed for such volatile anaesthetics as sevoflurane and desflurane.

The subsarcolemmal local Ca^{2+} releases from the SR with a resultant activation of forward mode Na^+/Ca^{2+} exchanger

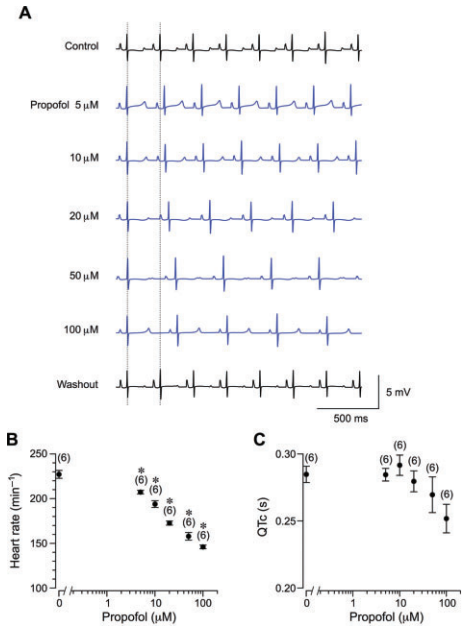

Figure 9

Negative chronotropic effect of propofol on Langendorff-perfused guinea pig hearts. (A) ECG recorded before (control), during administration of 5, 10, 20, 50 and 100 μM propofol in a cumulative manner (each concentration for approximately 5 min), and 8 min after washout. Two dotted vertical lines denote the time interval between two successive QRS complexes measured under control conditions. (B) Concentration-dependent reduction of the heart rate in Langendorff-perfused hearts by propofol. (C) QTc intervals in the absence and presence of propofol. *$P < 0.05$ compared with control.

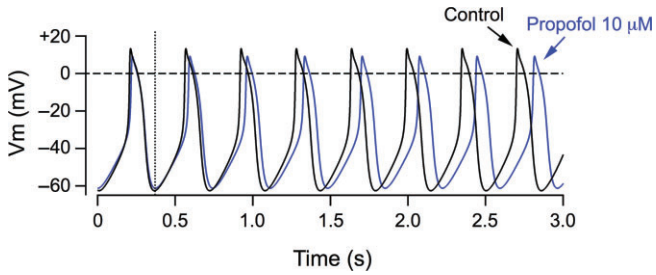

Figure 10

Computer simulation of negative chronotropic action of propofol on sinoatrial node automaticity. Spontaneous action potentials of the sinoatrial node cell model of Maltsev–Lakatta under control conditions (black) and in the presence of 10 μM propofol (blue), obtained by incorporating the degree of conductance decreases in I_f (18.8%), $I_{Ca,T}$ (27.2%), $I_{Ca,L}$ (22.5%), I_{Kr} (3.5%) and I_{Ks} (22.5%), obtained by the patch-clamp experiments, into the model. The spontaneous action potentials in control and in the presence of 10 μM propofol are superimposed at the time points of MDP of the first action potentials, as indicated by the vertical dotted line.

(NCX) play a central role in Ca^{2+} clock mechanism of sinoatrial node automaticity (Bogdanov *et al.*, 2006; Lakatta *et al.*, 2010). Although there is little information concerning the direct effect of propofol on SR Ca^{2+} release in cardiomyocytes, it is reasonable to expect that SR Ca^{2+} release is decreased following the reduction of Ca^{2+} influx through $I_{Ca,L}$ (Mangoni *et al.*, 2006a). In addition, propofol has been shown to inhibit forward mode NCX in heart cells (Wickley *et al.*, 2007). Taken together, possible reductions of forward mode NCX activity caused by propofol can be involved in the mechanisms underlying the negative chronotropic action of propofol.

It has yet to be fully understood whether the inhibition of I_f, $I_{Ca,T}$, $I_{Ca,L}$ and I_{Ks} by propofol is due to direct binding to the channel proteins or indirect interaction with the modulatory proteins and/or lipid bilayers in which channel proteins are embedded. Future studies should examine the precise mechanisms involved in the inhibitor action of propofol on these currents.

The present experiments provide electrophysiological evidence that propofol produces a direct negative chronotropic effect on guinea pig sinoatrial node pacemaker cells. Cardiac ion channel expression is rather similar between humans and guinea pigs, with the exception of the transient outward K^+ current (I_{to}), although there are some functional differences in ionic currents including I_{Ks} between these two species (Heath and Terrar, 1996b; Jost *et al.*, 2007). The guinea pig has therefore been used as an animal model in many studies to investigate the effect of preclinical and clinical drugs on ECG, cardiac contractility and haemodynamics (Yao *et al.*, 2008; Mooney *et al.*, 2012; Morissette *et al.*, 2013). However, because information is limited regarding the ionic mechanisms underlying the sinoatrial node automaticity in humans (Verkerk *et al.*, 2007), it still remains unclear as to whether the present experimental findings obtained from guinea pig sinoatrial node cells can be directly extrapolated to man.

A previous study using the patch-clamp technique and Langendorff perfusion system has demonstrated that adult guinea pigs do not display gender differences in (i) function and density of various ionic currents in ventricular myocytes, such as $I_{Ca,L}$, I_{Kr} and I_{Ks}; (ii) action potential parameters; and (iii) heart rate and other ECG parameters including QTc intervals (Brouillette *et al.*, 2007). However, there is no information concerning the possible gender difference in ionic currents in sinoatrial node cells of the guinea pig. It is also well recognized that cardiac ion channels are affected by sex steroid hormones, such as oestrogen and androgen (Tadros *et al.*, 2014). It is therefore ideal to conduct experiments using both genders of animal models to check the possible gender differences in the response to propofol.

There is evidence that propofol has a potential effect on the autonomic nervous system (Ebert *et al.*, 1992), which densely innervates the heart to regulate various cardiac functions, such as sinoatrial node automaticity, atrioventricular conduction velocity and myocardial contractility. Because heart rate is determined by the complex interaction of sympathetic and parasympathetic activities with intrinsic sinoatrial node automaticity, the relative balance between sympathetic and parasympathetic tone is an important modulatory factor in the control of the heart rate *in vivo* (Mangoni and Nargeot, 2008). Spectral analyses of heart rate variability in patients have shown that propofol anaesthesia reduces parasympathetic tone to a lesser degree than sympathetic tone, leading to parasympathetic dominance accompanied by bradycardia (Kanaya *et al.*, 2003). In this way, the

effect of propofol on the autonomic nervous system should also be taken into consideration to explain the changes in heart rate under propofol anaesthesia.

In conclusion, micromolar concentrations of propofol suppress multiple ionic currents and decelerate the spontaneous activity of the cardiac primary pacemaker sinoatrial node. These findings may therefore provide an important electrophysiological basis for the insight into the mechanisms underlying the propofol-induced bradycardia in the clinical setting.

Acknowledgements

This study was supported by a Grant-in-Aid for Young Scientists (B) (No. 24791590 to Akiko Kojima) and a Grant-in-Aid for Scientific Research (C) (No. 24592335 to Hirotoshi Kitagawa and Nos. 24591086 and 25460287 to Hiroshi Matsuura) from the Japan Society for the Promotion of Science (Tokyo, Japan).

Author contributions

A. K. and H. M. designed and performed the experiments. A. K., Y. I. and H. M. analysed the data. A. K., Y. I., H. K. and H. M. participated in the data interpretation. A. K. and H. M. wrote the manuscript. A. K., Y. I., H. K. and H. M. approved the final manuscript.

Conflicts of interest

None.

References

Alexander SPH, Benson HE, Faccenda E, Pawson AJ, Sharman JL, Spedding M *et al.* (2013a). The Concise Guide to PHARMACOLOGY 2013/14: G protein-coupled receptors. Br J Pharmacol 170: 1459–1581.

Alexander SPH, Benson HE, Faccenda E, Pawson AJ, Sharman JL, Spedding M *et al.* (2013b). The Concise Guide to PHARMACOLOGY 2013/14: Ion channels. Br J Pharmacol 170: 1607–1651.

Alexander SPH, Benson HE, Faccenda E, Pawson AJ, Sharman JL, Spedding M *et al.* (2013c). The Concise Guide to PHARMACOLOGY 2013/14: Transporters. Br J Pharmacol 170: 1706–1796

Alphin RS, Martens JR, Dennis DM (1995). Frequency-dependent effects of propofol on atrioventricular nodal conduction in guinea pig isolated heart. Mechanism and potential antidysrhythmic properties. Anesthesiology 83: 382–394.

Baig SM, Koschak A, Lieb A, Gebhart M, Dafinger C, Nürnberg G *et al.* (2011). Loss of $Ca_V1.3$ (*CACNA1D*) function in a human channelopathy with bradycardia and congenital deafness. Nat Neurosci 14: 77–84.

Baraka A (1988). Severe bradycardia following propofol-suxamethonium sequence. Br J Anaesth 61: 482–483.

Baruscotti M, Bucchi A, Viscomi C, Mandelli G, Consalez G, Gnecchi-Rusconi T *et al.* (2011). Deep bradycardia and heart block caused by inducible cardiac-specific knockout of the pacemaker channel gene HCN4. Proc Natl Acad Sci U S A 108: 1705–1710.

Bogdanov KY, Maltsev VA, Vinogradova TM, Lyashkov AE, Spurgeon HA, Stern MD *et al.* (2006). Membrane potential fluctuations resulting from submembrane Ca^{2+} releases in rabbit sinoatrial nodal cells impart an exponential phase to the late diastolic depolarization that controls their chronotropic state. Circ Res 99: 979–987.

Boyett MR, Honjo H, Kodama I (2000). The sinoatrial node, a heterogeneous pacemaker structure. Cardiovasc Res 47: 658–687.

Brouillette J, Lupien MA, St-Michel C, Fiset C (2007). Characterization of ventricular repolarization in male and female guinea pigs. J Mol Cell Cardiol 42: 357–366.

Cacheaux LP, Topf N, Tibbs GR, Schaefer UR, Levi R, Harrison NL *et al.* (2005). Impairment of hyperpolarization-activated, cyclic nucleotide-gated channel function by the intravenous general anesthetic propofol. J Pharmacol Exp Ther 315: 517–525.

Chandler NJ, Greener ID, Tellez JO, Inada S, Musa H, Molenaar P *et al.* (2009). Molecular architecture of the human sinus node: insights into the function of the cardiac pacemaker. Circulation 119: 1562–1575.

Chen X, Shu S, Bayliss DA (2005). Suppression of I_h contributes to propofol-induced inhibition of mouse cortical pyramidal neurons. J Neurophysiol 94: 3872–3883.

Colson P, Barlet H, Roquefeuill B, Eledjam JJ (1988). Mechanism of propofol bradycardia. Anesth Analg 67: 906–907.

Cullen PM, Turtle M, Prys-Roberts C, Way WL, Dye J (1987). Effect of propofol anesthesia on baroreflex activity in humans. Anesth Analg 66: 1115–1120.

Dawidowicz AL, Kalitynski R, Fijalkowska A (2003). Free and bound propofol concentrations in human cerebrospinal fluid. Br J Clin Pharmacol 56: 545–550.

DiFrancesco D (1993). Pacemaker mechanisms in cardiac tissue. Annu Rev Physiol 55: 455–472.

Dobrzynski H, Boyett MR, Anderson RH (2007). New insights into pacemaker activity: promoting understanding of sick sinus syndrome. Circulation 115: 1921–1932.

Dorrington KL (1989). Asystole with convulsion following a subanesthetic dose of propofol plus fentanyl. Anaesthesia 44: 658–659.

Ebert TJ, Muzi M, Berens R, Goff D, Kampine JP (1992). Sympathetic responses to induction of anesthesia in humans with propofol or etomidate. Anesthesiology 76: 725–733.

Ebert TJ, Harkin CP, Muzi M (1995). Cardiovascular responses to sevoflurane: a review. Anesth Analg 81 (Suppl. 6): S11–S22.

Franks NP (2008). General anaesthesia: from molecular targets to neuronal pathways of sleep and arousal. Nat Rev Neurosci 9: 370–386.

Ganansia M-F, Francois TP, Ormezzano X, Pinaud ML, Lepage JY (1989). Atrioventricular Mobitz I block during propofol anesthesia for laparoscopic tubal ligation. Anesth Analg 69: 524–525.

Gao Z, Chen B, Joiner ML, Wu Y, Guan X, Koval OM *et al.* (2010). I_f and SR Ca^{2+} release both contribute to pacemaker activity in canine sinoatrial node cells. J Mol Cell Cardiol 49: 33–40.

Hagiwara N, Irisawa H, Kameyama M (1988). Contribution of two types of calcium currents to the pacemaker potentials of rabbit sino-atrial node cells. J Physiol 395: 233–253.

Heath BM, Terrar DA (1996a). Separation of the components of the delayed rectifier potassium current using selective blockers of I_{Kr} and I_{Ks} in guinea-pig isolated ventricular myocytes. Exp Physiol 81: 587–603.

Heath BM, Terrar DA (1996b). The deactivation kinetics of the delayed rectifier components I_{Kr} and I_{Ks} in guinea-pig isolated ventricular myocytes. Exp Physiol 81: 605–621.

Hemmings HC Jr, Akabas MH, Goldstein PA, Trudell JR, Orser BA, Harrison NL (2005). Emerging molecular mechanisms of general anesthetic action. Trends Pharmacol Sci 26: 503–510.

Jost N, Papp JG, Varró A (2007). Slow delayed rectifier potassium current (I_{Ks}) and the repolarization reserve. Ann Noninvasive Electrocardiol 12: 64–78.

Kanaya N, Hirata N, Kurosawa S, Nakayama M, Namiki A (2003). Differential effects of propofol and sevoflurane on heart rate variability. Anesthesiology 98: 34–40.

Kilkenny C, Browne W, Cuthill IC, Emerson M, Altman DG (2010). Animal research: reporting *in vivo* experiments: the ARRIVE guidelines. Br J Pharmacol 160: 1577–1579.

Kojima A, Kitagawa H, Omatsu-Kanbe M, Matsuura H, Nosaka S (2012). Inhibitory effects of sevoflurane on pacemaking activity of sinoatrial node cells in guinea-pig heart. Br J Pharmacol 166: 2117–2135.

Kojima A, Ito Y, Kitagawa H, Matsuura H, Nosaka S (2013). Remifentanil has a minimal direct effect on sinoatrial node pacemaker activity in the guinea pig heart. Anesth Analg 117: 1072–1077.

Kojima A, Ito Y, Kitagawa H, Matsuura H, Nosaka S (2014). Direct negative chronotropic action of desflurane on sinoatrial node pacemaker activity in the guinea pig heart. Anesthesiology 120: 1400–1413.

Komatsu R, Turan AM, Orhan-Sungur M, McGuire J, Radke OC, Apfel CC (2007). Remifentanil for general anaesthesia: a systematic review. Anaesthesia 62: 1266–1280.

Lakatta EG, Maltsev VA, Vinogradova TM (2010). A coupled SYSTEM of intracellular Ca^{2+} clocks and surface membrane voltage clocks controls the timekeeping mechanism of the heart's pacemaker. Circ Res 106: 659–673.

Lei M, Brown HF (1996). Two components of the delayed rectifier potassium current, I_K, in rabbit sino-atrial node cells. Exp Physiol 81: 725–741.

Maltsev VA, Lakatta EG (2009). Synergism of coupled subsarcolemmal Ca^{2+} clocks and sarcolemmal voltage clocks confers robust and flexible pacemaker function in a novel pacemaker cell model. Am J Physiol 296: H594–H615.

Mangoni ME, Nargeot J (2008). Genesis and regulation of the heart automaticity. Physiol Rev 88: 919–982.

Mangoni ME, Couette B, Bourinet E, Platzer J, Reimer D, Striessnig J *et al*. (2003). Functional role of L-type $Ca_V1.3$ Ca^{2+} channels in cardiac pacemaker activity. Proc Natl Acad Sci USA 100: 5543–5548.

Mangoni ME, Couette B, Marger L, Bourinet E, Striessnig J, Nargeot J (2006a). Voltage-dependent calcium channels and cardiac pacemaker activity: from ionic currents to genes. Prog Biophys Mol Biol 90: 38–63.

Mangoni ME, Traboulsie A, Leoni AL, Couette B, Marger L, Le Quang K *et al*. (2006b). Bradycardia and slowing of the atrioventricular conduction in mice lacking $Ca_V3.1/\alpha_{1G}$ T-type calcium channels. Circ Res 98: 1422–1430.

Matsuura H, Ehara T, Ding WG, Omatsu-Kanbe M, Isono T (2002). Rapidly and slowly activating components of delayed rectifier K^+ current in guinea-pig sino-atrial node pacemaker cells. J Physiol 540: 815–830.

McGrath JC, Drummond GB, McLachlan EM, Kilkenny C, Wainwright CL (2010). Guidelines for reporting experiments involving animals: the ARRIVE guidelines. Br J Pharmacol 160: 1573–1576.

Milanesi R, Baruscotti M, Gnecchi-Ruscone T, DiFrancesco D (2006). Familial sinus bradycardia associated with a mutation in the cardiac pacemaker channel. N Engl J Med 354: 151–157.

Mooney L, Marks L, Philp KL, Skinner M, Coker SJ, Currie S (2012). Optimising conditions for studying the acute effects of drugs on indices of cardiac contractility and on haemodynamics in anaesthetized guinea pigs. J Pharmacol Toxicol Methods 66: 43–51.

Morissette P, Nishida M, Trepakova E, Imredy J, Lagrutta A, Chaves A *et al*. (2013). The anesthetized guinea pig: an effective early cardiovascular derisking and lead optimization model. J Pharmacol Toxicol Methods 68: 137–149.

Pawson AJ, Sharman JL, Benson HE, Faccenda E, Alexander SP, Buneman OP *et al*.; NC-IUPHAR (2014). The IUPHAR/BPS Guide to PHARMACOLOGY: an expert-driven knowledgebase of drug targets and their ligands. Nucl Acids Res 42 (Database Issue): D1098–D1106.

Postea O, Biel M (2011). Exploring HCN channels as novel drug targets. Nat Rev Drug Discov 10: 903–914.

Sarai N, Matsuoka S, Noma A (2006). *simBio*: a Java package for the development of detailed cell models. Prog Biophys Mol Biol 90: 360–377.

Shibata S, Ono K, Iijima T (2004). Sevoflurane inhibition of the slowly activating delayed rectifier K^+ current in guinea pig ventricular cells. J Pharmacol Sci 95: 363–373.

Smith I, White PF, Nathanson M, Gouldson R (1994). Propofol. An update on its clinical use. Anesthesiology 81: 1005–1043.

Stowe DF, Bosnjak ZJ, Kampine JP (1992). Comparison of etomidate, ketamine, midazolam, propofol, and thiopental on function and metabolism of isolated hearts. Anesth Analg 74: 547–558.

Tadros R, Ton AT, Fiset C, Nattel S (2014). Sex differences in cardiac electrophysiology and clinical arrhythmias: epidemiology, therapeutics, and mechanisms. Can J Cardiol 30: 783–792.

Tellez JO, Dobrzynski H, Greener ID, Graham GM, Laing E, Honjo H *et al*. (2006). Differential expression of ion channel transcripts in atrial muscle and sinoatrial node in rabbit. Circ Res 99: 1384–1393.

Thomas GP, Gerlach U, Antzelevitch C (2003). HMR 1556, a potent and selective blocker of slowly activating delayed rectifier potassium current. J Cardiovasc Pharmacol 41: 140–147.

Tibbs GR, Rowley TJ, Sanford RL, Herold KF, Proekt A, Hemmings HC Jr *et al*. (2013). HCN1 channels as targets for anesthetic and nonanesthetic propofol analogs in the amelioration of mechanical and thermal hyperalgesia in a mouse model of neuropathic pain. J Pharmacol Exp Ther 345: 363–373.

Todorovic SM, Perez-Reyes E, Lingle CJ (2000). Anticonvulsants but not general anesthetics have differential blocking effects on different T-type current variants. Mol Pharmacol 58: 98–108.

Tramèr MR, Moore RA, McQuay HJ (1997). Propofol and bradycardia: causation, frequency and severity. Br J Anaesth 78: 642–651.

Verheijck EE, van Ginneken AC, Bourier J, Bouman LN (1995). Effects of delayed rectifier current blockade by E-4031 on impulse generation in single sinoatrial nodal myocytes of the rabbit. Circ Res 76: 607–615.

Verkerk AO, Wilders R, van Borren MM, Peters RJ, Broekhuis E, Lam K *et al*. (2007). Pacemaker current (I_f) in the human sinoatrial node. Eur Heart J 28: 2472–2478.

Wickley PJ, Shiga T, Murray PA, Damron DS (2007). Propofol modulates Na^+-Ca^{2+} exchange activity *via* activation of protein kinase C in diabetic cardiomyocytes. Anesthesiology 106: 302–311.

Wu MH, Su MJ, Sun SS (1997). Comparative direct electrophysiological effects of propofol on the conduction system and ionic channels of rabbit hearts. Br J Pharmacol 121: 617–624.

Yamamoto S, Kawana S, Miyamoto A, Ohshika H, Namiki A (1999). Propofol-induced depression of cultured rat ventricular myocytes is related to the M_2-acetylcholine receptor-NO-cGMP signaling pathway. Anesthesiology 91: 1712–1719.

Yang CY, Wong CS, Yu CC, Luk HN, Lin CI (1996). Propofol inhibits cardiac L-type calcium current in guinea pig ventricular myocytes. Anesthesiology 84: 626–635.

Yao X, Anderson DL, Ross SA, Lang DG, Desai BZ, Cooper DC *et al*. (2008). Predicting QT prolongation in humans during early drug development using hERG inhibition and an anaesthetized guinea-pig model. Br J Pharmacol 154: 1446–1456.

Ying SW, Abbas SY, Harrison NL, Goldstein PA (2006). Propofol block of I_h contributes to the suppression of neuronal excitability and rhythmic burst firing in thalamocortical neurons. Eur J Neurosci 23: 465–480.

Young ME, Razeghi P, Cedars AM, Guthrie PH, Taegtmeyer H (2001). Intrinsic diurnal variations in cardiac metabolism and contractile function. Circ Res 89: 1199–1208.